**Asian Journal of Andrology (2024) 26,** 212–219
www.asiaandro.com; https://journals.lww.com/ajandrology

*Open Access*

**ORIGINAL ARTICLE**

Sperm Biology

# Pyruvate kinase M in germ cells is essential for sperm motility and male fertility but not spermatogenesis

**Gao-Qing Qian[1,*], Xiao-Chen Wang[2,*], Xi Zhang[3], Bin Shen[1], Qiang Liu[2]**

**Male germ cells employ specific metabolic pathways throughout their developmental stages. In a previous study, we discovered heightened expression of pyruvate kinase M (PKM), a pivotal glycolytic enzyme, in spermatogonia and spermatids. To gain deeper insights into PKM's roles in spermatogenesis, sperm function, and male fertility, we engineered a conditional-knockout mouse model (*Pkm*-vKO mice) to selectively disrupt the *Pkm* gene within germ cells. Despite maintaining regular testicular histology and sperm morphology, the male *Pkm*-vKO mice were infertility, characterized by significant impairments in sperm motility and adenosine triphosphate (ATP) generation. In addition, *Pkm*-null spermatozoa exhibited similar deficits in protein tyrosine phosphorylation linked to capacitation, as well as compromised performance in *in vitro* fertilization experiments. To conclude, PKM's presence is not obligatory for the entirety of spermatogenesis in male germ cells; however, it emerges as a critical factor influencing sperm motility and overall male fertility.**

*Asian Journal of Andrology* (2024) **26**, 212–219; doi: 10.4103/aja202350; published online: 24 October 2023

**Keywords:** glycolysis; male fertility; pyruvate kinase M; sperm motility; spermatogenesis

## INTRODUCTION

Spermatogenesis is a multifaceted developmental journey encompassing mitosis, meiosis, and spermatogenesis. This intricate process culminates in the maturation of spermatozoa, characterized by their distinctive structure comprising a head and tail.[1] In mammals, spermatogonial stem cells (SSCs) exhibit a dual behavior: they can either engage in self-renewal or embark on successive rounds of mitotic divisions, leading to the formation of A paired (Apr) and A aligned (Aal) spermatogonia.[2] Aal spermatogonia transition into A1 spermatogonia and further progress through a series of mitotic divisions to eventually develop into type B spermatogonia. These type B spermatogonia then proceed to generate primary spermatocytes, entering the phase of meiosis. In this phase, there is a combination of reduced division and genetic recombination, leading to the formation of haploid round spermatids. Subsequently, during the process of spermiogenesis, these round spermatids undergo intricate morphological and biochemical changes, ultimately maturing into elongated and fully developed spermatozoa. This journey involves a precise sequence of spatial and temporal transformations, including nucleus condensation, acrosome and flagella formation, which are meticulously orchestrated and dynamically regulated.[3,4]

Testicular spermatozoa are inherently nonfunctional and lack the capability for natural oocyte fertilization. Their capacity for fertilization and forward motility characteristics must be acquired as they undergo transit within the epididymis.[5,6] On ejaculation, newly released spermatozoa undergo a vital process termed capacitation, followed by a subsequent morphological shift referred to as the acrosome reaction, within the female reproductive tract. Only after undergoing these changes are they poised to successfully fertilize eggs in the ampulla region of the oviduct.[7,8]

Spermatogenesis and the diverse functions of sperm demand substantial energy resources. This energy is primarily derived through two key metabolic pathways: glycolysis and mitochondrial oxidative phosphorylation (OXPHOS), which yield adenosine triphosphate (ATP). Mammalian spermatogonial stem cells (SSCs) reside in a hypoxic, avascular niche. Notably, it is hypothesized that SSC self-renewal and proliferation pivot on glycolysis, while spermatogonial differentiation hinges on mitochondrial respiration. As differentiation progresses, the energy production balance transitions from glycolysis to OXPHOS, catering to the increasing energy requirements.[9–11] The role of glycolysis and OXPHOS as ATP sources to sustain the motility of mammalian sperm has been a topic of longstanding debate spanning decades.[12–14] There is a prevailing notion that glycolysis significantly contributes to ATP production, vital for sustaining sperm motility.[15,16]

In an prior investigation, we scrutinized single-cell RNA sequencing data obtained from mouse testes.[17] On deeper analysis, a notable

[1]State Key Laboratory of Reproductive Medicine and Offspring Health, Nanjing Medical University, Nanjing 211166, China; [2]Shanghai Key Laboratory of Reproductive Medicine, Department of Histoembryology, Genetics and Developmental Biology, Shanghai Jiao Tong University School of Medicine, Shanghai 200025, China; [3]State Key Laboratory of Molecular Biology, Shanghai Key Laboratory of Molecular Andrology, Shanghai Institute of Biochemistry and Cell Biology, Center for Excellence in Molecular Cell Science, Chinese Academy of Sciences, University of Chinese Academy of Sciences, Shanghai 200031, China.
*These authors contributed equally to this work.
Correspondence: Dr. B Shen (binshen@njmu.edu.cn) or Dr. Q Liu (qliu0122@shsmu.edu.cn)
Received: 25 March 2023; Accepted: 16 August 2023

discovery emerged, which is pyruvate kinase M (PKM), a crucial enzyme within glycolysis, exhibited marked expression in spermatogonia and spermatids, revealing a distinctive pattern compared to spermatocytes (**Supplementary Figure 1**). During the conclusive stage of glycolysis, pyruvate kinase (PK) facilitates the conversion of adenosine diphosphate (ADP) and phosphoenolpyruvate into ATP and pyruvic acid. In addition, in anaerobic conditions, pyruvate has the potential to undergo oxidation, resulting in the production of lactic acid[18] (**Figure 1a**). In mammals, four pyruvate kinase isozymes (L, R, M1, and M2) exist, arising from two distinct genes: pyruvate kinase, liver and red blood cell (*Pklr*), and pyruvate kinase M (*Pkm*). The L and R isozymes stem from PKLR due to distinct RNA splicing, while PKM1 and PKM2 emerge through alternative splicing of PKM.[19,20] The L isotype predominates in the liver, R is prevalent in red blood cells, M1 is primarily present in muscle, heart, and brain tissues, while M2 was initially identified in early fetal tissues and is common among cancer cells. The *Pkm* gene spans approximately 32 Kb, encompassing 12 exons and 11 introns. The final mRNA product for the ultimate mRNA transcript for *PKM2* includes exon 10 while omitting exon 9, a distinctive feature unique to *PKM1*.[21] Diverging from other PK isoforms, PKM2 has been documented to intricately influence gene expression and serves as a kinase that phosphorylates proteins crucial for cellular growth and survival.[21,22]

In our pursuit to unravel the significance of the crucial glycolytic enzyme PKM in both spermatogenesis and male fertility, we engineered a conditional knockout mouse model through germline PKM deletion facilitated by *Vasa Cre* recombinase (*Vasa-Cre)*. Intriguingly, our findings revealed a paradox: despite germline deletion, the mice exhibited uninterrupted spermatogenesis. Nevertheless, a noteworthy outcome emerged that the affected animals encountered a decline in male fertility and a noticeable reduction in sperm motility.

## MATERIALS AND METHODS

### *Mice*

Clustered regularly interspaced short palindromic repeats (CRISPR)/CRISPR-associated protein 9 (Cas9) technology was employed to create the conditional mutant alleles for *Pkm*. The *Pkm*-floxed line, encompassing locus of crossover in P1 (*loxP*) sites flanking exons 4 and 5 of the *Pkm* gene, was established by microinjecting the CRISPR/Cas9 system and the donor into fertilized eggs of C57BL/6J mice. Positive F0 mice were obtained and their status was verified through the polymerase chain reaction (PCR) and sequencing. A stable F1 generation mouse model was generated by mating the positive F0 mice with C57BL/6J mice. For the targeted conditional deletion of *Pkm* in advanced germ cells, *Pkm*-floxed mice (GemPharmatech, Nanjing, China) were bred with the germ cell-specific *Vasa-Cre* mouse line (Jackson Laboratory, Bar Harbor, ME, USA). This breeding strategy led to the excision of *loxP*-flanked exon 4 and exon 5, resulting in the generation of germ cell-specific *Pkm* knockout mice. All mice utilized in the study were maintained on the C57BL/6J (B6) background, and all animal experiments adhered strictly to the guidelines and were approved by the Animal Care and Use Committee at the Shanghai Institute of Biochemistry and Cell Biology, Chinese Academy of Sciences (Shanghai, China; Approval No. 2021-121).

### *Sperm isolation and in vitro capacitation*

Spermatozoa were harvested from the cauda epididymidis of sexually mature mice (>8-week-old) in modified Krebs–Ringer medium (HM)

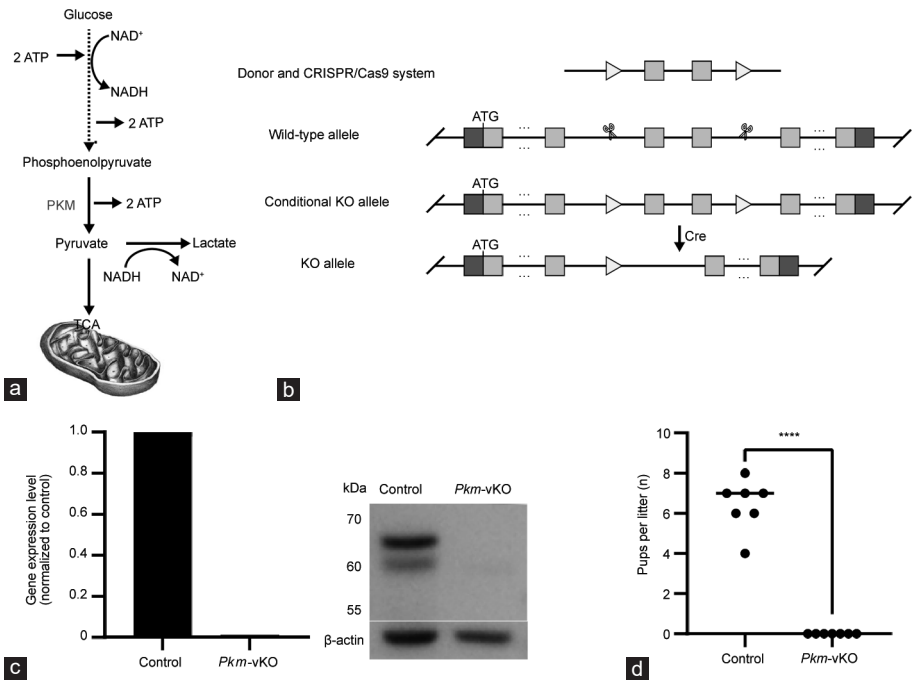


**Figure 1:** Targeted disruption of *Pkm* in germ cells. (**a**) Simplified diagram depicting glycolysis, emphasizing the essential role of PKM in ATP production through this pathway. (**b**) Schematic illustration outlining the strategy employed to generate *Pkm*-floxed line ($Pkm^{F/F}$) and *Pkm* cell-specific knockout (vKO) mice. The presence of *loxP* sites flanking exons 4 and 5 enables their excision by Cre recombinase. (**c**) Germ cell-specific elimination of PKM expression was observed. mRNA extracted from crude germ cells was quantitatively assessed using qRT-PCR in both control and *Pkm*-vKO mice. Furthermore, protein extracts from spermatozoa in control and *Pkm*-vKO mice were analyzed through western blot utilizing an antibody specific to PKM1/2. (**d**) Comprehensive statistical analysis of the fertility of male mice from both control and *Pkm*-vKO groups. $^{***}P < 0.001$. ATP: adenosine triphosphate; TCA: tricarboxylic acid; PKM: pyruvate kinase M; qRT-PCR: quantitative reverse transcription polymerase chain reaction; NADH: nicotinamide adenine dinucleotide; CRISPR/Cas9: clustered regularly interspaced short palindromic repeats/CRISPR-associated protein 9.

buffer, a refined Krebs–Ringer bicarbonate medium known as HM-HEPES buffered medium.[23,24] Using iris scissors, two to four incisions were carefully made in each cauda epididymidis, enabling the release of spermatozoa into the medium via 15-min incubation at 37°C in the environment composed of 5% $CO_2$ and air. Subsequently, the resulting sperm suspension was gently transferred to a 1.5 ml centrifuge tube (Eppendorf, Hamburg, Germany) and securely stored within a 5% $CO_2$ incubator at 37°C for subsequent use.

Portions of the remaining sperm suspension were diluted into HMB medium (HM supplemented with 0.05 mmol $l^{-1}$ sodium bicarbonate and 0.09 mmol $l^{-1}$ bovine serum albumin), followed by an incubation at 37°C in a setting comprising 5% $CO_2$ and air. This process allowed for the capacitation of spermatozoa in preparation for subsequent utilization.

***Histological and immunohistochemical analyses***

Testes were fixed in either Bouin's buffer or 4% paraformaldehyde (PFA), then embedded in paraffin and subsequently sectioned. The sections underwent deparaffinization, rehydration, and staining with hematoxylin and eosin (H and E).[25] For immunofluorescence analysis, sections were subjected to heat-induced antigen retrieval in 10 mmol $l^{-1}$ sodium citrate buffer (pH 6.0) for 15 min, followed by cooling to the room temperature and subsequent washing in phosphate-buffered saline (PBS) containing 0.1% Triton X-100. Subsequently, sections were obstructed using a solution comprising 10% normal donkey serum and 0.1% Triton X-100 in PBS, incubated for 60 min at room temperature and left to incubate overnight at 4°C with primary antibodies diluted in the obstructing solution (PKM1 and PKM2; Proteintech, Chicago, IL, USA). The next day, slides underwent four 15-min washes in PBS with 0.1% Triton X-100, followed by incubation with Alexa Fluor 488- and Alexa Fluor 594-conjugated donkey secondary antibodies (Jackson ImmunoResearch Laboratories, West Chester, PA, USA) at a 1:400 dilution. After 60 min at room temperature, sections were washed in PBS, briefly rinsed in pure ethanol, mounted in Prolong Gold Antifade medium containing 4',6-diamidino-2-phenylindole (DAPI; Molecular Probes, Cambridge, UK) and subjected to analysis via fluorescence microscopy.[3]

***Transmission electron microscopy***

The cauda epididymidis samples from both control and $Pkm^{F/\Delta}$-vKO ($Pkm^{fl/del}$, *Vasa-Cre*, germ cell-specific *Pkm* gene knockout) mice were immersed in 2.5% glutaraldehyde at 4°C overnight for fixation. Following three washes with 0.1 mol $l^{-1}$ phosphate buffer, the caudae underwent secondary fixation with 2% osmic acid for 1.5 h, followed by washing and dehydration through an ethanol gradient before embedding in plastic resin. Subsequently, ultra-thin sections measuring 70 nm in thickness were prepared using an EM UC6 ultramicrotome (Leica, Wetzlar, Germany). These thin sections were stained with 2% uranyl acetate for 15 min and 1% lead citrate for 5 min to enhance visibility during observation.

***RNA isolation and quantitative reverse transcription polymerase chain reaction (qRT-PCR)***

Total RNA was extracted with Trizol reagent (15596-026; Life Technologies, Carlsbad, CA, USA), followed by cDNA synthesis from the total RNA with a Takara RT reagent kit with gDNA Eraser (Takara Biomedical Technology, Beijing, China). The expression of the *Pkm* gene was assessed via PCR, employing the following primer pairs: forward primer 5'-GCATCTGATCCCATTCTCTAC-3' and reverse primer 5'-GTTCTCGTCACACTTCTCCAT-3'. For the control *β-actin*, the following primers were utilized: forward primer 5'-GCCCTCGTAGATGGGCACAG-3' and reverse primer 5'-TGTTACCAACTGGGACGAC-3'.

***Western blot***

Total proteins were extracted from spermatozoa of both control and $Pkm^{F/\Delta}$-vKO mice using sodium dodecyl sulfate-polyacrylamide gel electrophoresis (SDS-PAGE) on 10% polyacrylamide gels, followed by transfer onto nitrocellulose (NC) membranes. These membranes were then subjected to incubation with a mouse monoclonal antibody targeting phosphotyrosine (1:2500; Merck Millipore, Darmstadt, Germany), as well as a rabbit monoclonal antibody against PKM1/2 (1:1000; mAb #3190; Cell Signaling Technology, Danvers, MA, USA) at 4°C. Following three tris-buffered saline with 0.1% Tween 20 (TBST) washes, the membranes were exposed to affinity-purified goat anti-rabbit IgG or goat anti-mouse IgG + IgM, both conjugated to horseradish peroxidase (1:30 000; Kirkegaard and Perry Laboratories, Gaithersburg, MD, USA), for 1 h incubation. Ultimately, chemiluminescent peroxidase substrate (Amersham, Berkshire, UK) was utilized for the detection of immunoreactivity.

***Analysis of sperm motility***

Having gathered cauda epididymal spermatozoa in HM, small portions were diluted into HMB medium, aiming for a final concentration of approximately $10 \times 10^6$–$15 \times 10^6$ cells per ml. Subsequently, these prepared samples were subjected to an incubation period at 37°C, with a mixture of 5% $CO_2$ and air, spanning a duration of 1.5 h. The evaluation of sperm motility was conducted at 30-min intervals, utilizing computer-assisted sperm analysis (CASA) facilitated by Hamilton Thorne (Beverly, MA, USA). The CASA system comprehensively assessed various parameters, including curvilinear velocity (VCL), average path velocity (VAP), straight line velocity (VSL), amplitude of lateral head displacement (ALH), beat cross frequency (BCF), linearity (LIN), as well as other pertinent factors.[26] For every time interval, spermatozoa were gently mixed by creating a swirling motion, and an approximately 20 μl portion was carefully introduced into the CASA counting chamber (Hamilton Thorne, Beaverton, Ontario, Canada) through the utilization of a broad-bore pipette. Extending the analysis, over 200 cells were meticulously scrutinized from each animal during every individual time interval.

***Sperm viability***

The sperm suspension was meticulously blended with an equivalent volume of eosin-aniline black staining solution, followed by 30 s incubation for staining. Poststaining, 10 μl of this mixture was delicately applied onto a glass slide, allowing it to naturally air-dry. In each replicate, a minimum of 200 spermatozoa underwent thorough examination using brightfield optics. Under the microscope, sperm heads exhibiting white and pink hues were identified as live cells featuring an intact plasma membrane. Conversely, those sperm heads displaying a red hue were categorized as deceased cells with compromised plasma membranes.[27]

***Acrosome reaction***

Following a 60-min period of *in vitro* capacitation, the spermatozoa underwent extended incubation for an extra 30 min within the same medium, supplemented either with 10 μmol $l^{-1}$ A23187 calcium ionophore or 10 μmol $l^{-1}$ progesterone (Sigma-Aldrich, St. Louis, MO, USA) to trigger the acrosome reaction. In contrast, the control samples were exclusively exposed to the dimethyl sulfoxide (DMSO) solvent. After treatment, the sperm were subjected to fixation and stained using Coomassie Blue G-250 (Solarbio, Beijing, China) in accordance with

previous methodologies.[28,29] At least 200 cells were counted for every sample, wherein the evaluation focused on determining the occurrence or absence of deep blue staining within the acrosomal crescent situated on the anterior facet of the sperm head. Subsequently, the proportions of acrosome reactions triggered by A23187 and progesterone (Sigma-Aldrich, St. Louis, MO, USA) were calculated, adjusting for the baseline levels noted in the DMSO controls.

***Sperm ATP levels***

After undergoing incubation in HMB medium at a temperature of 37°C, in the environment comprised of 5% $CO_2$ and air, the spermatozoa were subjected to centrifugation at 500*g* for a duration of 5 min (5702R; Eppendorf). After removal of excess medium, the remaining 50 µl of suspension was resuspended and subsequently transferred to a tube containing an equivalent volume of lysate. This combined mixture was then placed on ice, permitting 10-min incubation, after which centrifugation at 12 000*g* was executed for 5 min, effectively gathering the supernatant. For ATP measurement, duplicate 50-µl aliquots of the supernatant were employed, utilizing a luciferase bioluminescence assay in accordance with the manufacturer's instructions (Enhanced ATP Assay Kit; Beyotime, Shanghai, China).

***Fertility assay***

Each individual *Pkm*-vKO male mouse was paired with two female mice aged 6 weeks each, for the initial month, followed by a subsequent month with a distinct pair of female mice. Over the course of the mating period, careful observation was extended to all female mice for an additional month. After birth, a thorough assessment encompassing the count, viability, and dimensions of offspring within each litter was meticulously conducted and documented. The *in vitro* fertilization (IVF) process was executed in accordance with established procedures, as previously outlined,[30] ascertained by enumerating the quantity of two-cell embryos following a 24-h incubation period.

***Isolation of spermatogenic cells***

To enrich spermatogenic cells, a method involving fluorescence-activated cell sorting (FACS) utilizing Hoechst 33342 dye (Sigma-Aldrich, Darmstadt, Germany) was employed. Adult testes were carefully collected in PBS and maintained on ice. Following the removal of the tunica albuginea, the seminiferous tubules underwent digestion in PBS supplemented with 120 units per ml of collagenase type I (Worthington, Rutland, VT, USA). Subsequently, the tubules were subjected to further digestion with 0.25% trypsin (Gibco, Wilmington, MA, USA) and 5 mg $ml^{-1}$ DNaseI (Gibco), with the reaction being halted by the introduction of fetal bovine serum (FBS). The resulting dissociated testicular cell suspension was gathered and subsequently resuspended in DMEM containing 0.1 mg $ml^{-1}$ of DNaseI. Following a 30-min staining period with Hoechst 33 342, flow cytometric analysis was employed to facilitate the sorting of spermatogenic cells.

***Statistical analyses***

Statistical analysis was carried out employing GraphPad Prism 8 (GraphPad Software, La Jolla, CA, USA). Each experiment was conducted across a minimum of two replicates, with the outcomes being expressed as mean values accompanied by the standard deviation (s.d.). For the assessment of statistical significance, two-tailed, unpaired *t*-tests were utilized. Notably, differences yielding $P < 0.05$ were regarded as indicative of statistical significance.

## RESULTS

***Gene targeting and PKM expression in germ cells***

We delved into the dynamic expression patterns of PKM transcripts through a combination of testicular single-cell RNA sequencing data[17] and immunofluorescence analysis. Notably, PKM exhibited pronounced expression within spermatogonia and spermatids, standing in stark contrast to its levels in spermatocytes (**Supplementary Figure 1** and **2**). Following this, we employed the CRISPR/Cas9 system to establish a *Pkm*-floxed line (**Figure 1b**). These *Pkm*-floxed mice were then strategically bred with the *Vasa-Cre* mouse line, yielding *Pkm*-vKO mice. This specific breeding led to the targeted inactivation of *Pkm* within male germ cells, an effect that manifested as early as embryonic day 15 (E15).[31] Through qRT-PCR and western blot analyses, we unveiled a remarkable reduction in the expression of PKM transcripts and proteins within male germ cells of *Pkm*-vKO mice, nearly rendering them undetectable (**Figure 1c**). Immunostaining provided additional validation, affirming the absence of PKM proteins within male germ cells (**Supplementary Figure 2**). Subsequent mating experiments unequivocally demonstrated the infertility of male *Pkm*-vKO mice, firmly establishing the indispensability of PKM within germ cells for male fertility (**Figure 1d**). Subsequent to this, we conducted a thorough phenotype analysis to shed light on the underlying reasons behind the male infertility observed in the *Pkm*-vKO mice.

***Loss of PKM and testicular histology, sperm counts, and sperm ultrastructure***

Both *Pkm*-vKO males and their control counterparts displayed indistinguishable appearances and behaviors while also exhibiting comparable measures in terms of body weight, testis weight, and the count of cauda epididymal spermatozoa (**Figure 2a** and **2b**). Furthermore, no discernible distinctions emerged in terms of testicular histology between the control and *Pkm*-vKO mice **(Figure 2c**). Sperm ultrastructure was meticulously evaluated through transmission electron microscopy, revealing no discernible disparities between spermatozoa originating from both control and *Pkm*-vKO mice (**Supplementary Figure 3**). The fibrous sheath, outer dense fibers, central axoneme, and sperm head appeared normal in spermatozoa lacking PKM.

***PKM and normal sperm motility***

In the pursuit of understanding PKM's impact on sperm motility, we altered the incubation medium of the sperm by eliminating pyruvate, the direct product of PKM, and lactic acid, derived from pyruvate, from the initial HM and HMB medium. This left glucose as the exclusive energy source for the sperm. Spermatozoa from *Pkm*-vKO males displayed profound defects in motility. CASA was employed to evaluate the quantitative aspects of sperm motility promptly after collection (**Figure 3a**) and at 30-min intervals during incubation in HMB medium lacking pyruvate or lactic acid (**Figure 3b**). While most spermatozoa from both control and *Pkm*-vKO males exhibited some movement immediately after collection from the cauda epididymidis, the flagellar frequency and amplitude of spermatozoa lacking PKM were quite low, resulting in little forward movement compared with the vigorous progressive motility of control spermatozoa (**Figure 4a** and **4b**). The control spermatozoa retained vigorous motility over a 90-min incubation period, whereas those from *Pkm*-vKO mice almost lost their motility and forward movement after only 30 min of incubation under capacitating conditions (**Figure 4b**). The sperm motility loss could be partially restored by pyruvate and lactic acid supplementation, but the forward movement of PKM-deficient spermatozoa was not restored after substrate supplementation (**Figure 4c**).

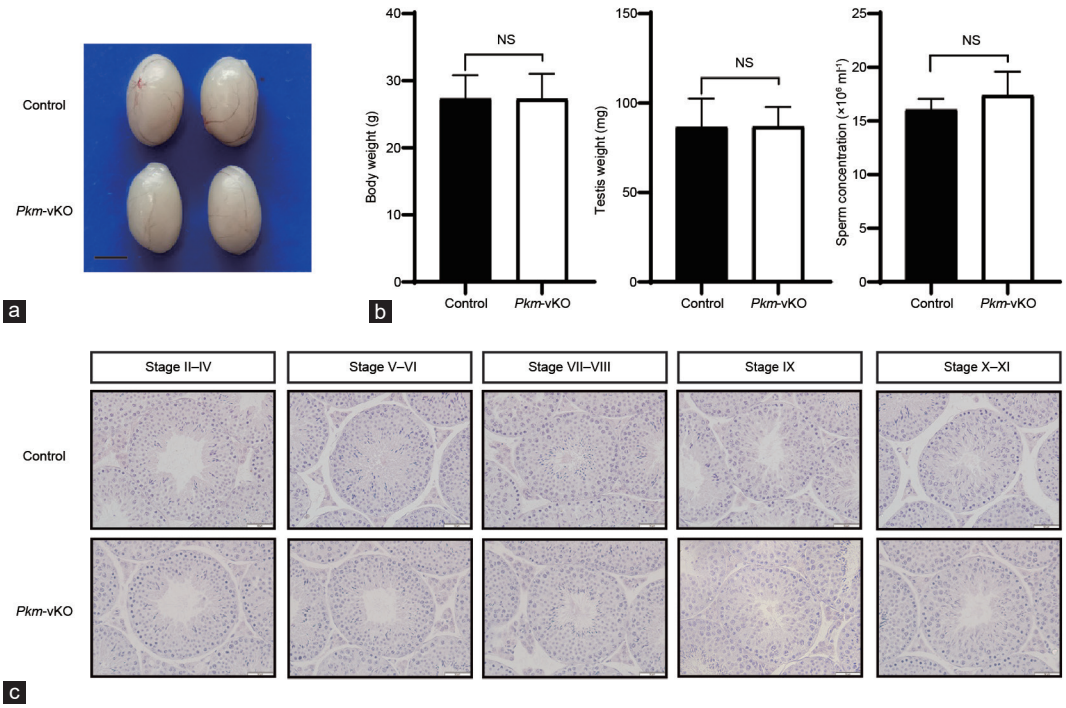


**Figure 2:** Impact of *Pkm* deletion on testis histology. (**a**) Visual representation showcasing the macroscopic appearance of representative testes derived from both control and *Pkm*-vKO mice. Scale bar = 3 mm. (**b**) Comparative analysis of body weight ($n$ = 5), testis weight ($n$ = 5), and sperm concentration in the cauda epididymidis ($n$ = 3) between control and *Pkm*-vKO mice. (**c**) Hematoxylin and eosin staining of select testicular sections obtained from control and *Pkm*-vKO mice ($n$=5 for each group), providing insights into histological changes. Scale bars = 50 μm. Results are displayed as mean ± standard deviation. Statistical significance was evaluated employing a two-tailed Student's $t$-test. PKM: pyruvate kinase M; *Pkm*-vKO: germ cell-specific *Pkm* gene knockout; NS: nonsignificant.

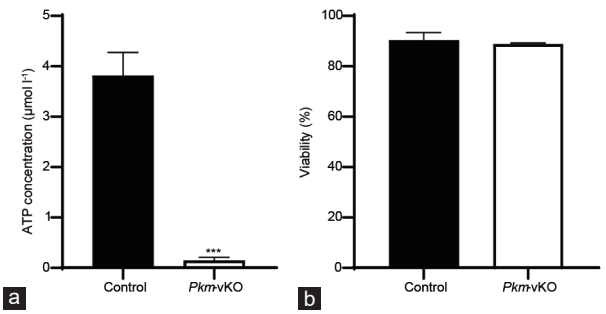


**Figure 3:** *Pkm* knockout undermines ATP production while sustaining sperm viability in HMB medium without pyruvate or lactic acid. (**a**) ATP production quantification was conducted on caudal epididymal spermatozoa ($n$ = 3). (**b**) The percentages of live and dead spermatozoa were determined and analyzed from eosin-aniline black staining ($n$ = 3). Results are presented as mean ± standard deviation. The $P$ value was calculated by two-tailed Student's $t$-test. $^{***}P < 0.001$. ATP: adenosine triphosphate; *Pkm*-vKO: germ cell-specific *Pkm* gene knockout.

### *ATP levels in spermatozoa lacking PKM*

Given that PKM plays a crucial role in the terminal phase of glycolysis, we closely monitored ATP levels in spermatozoa exposed to capacitating conditions within HMB medium, devoid of pyruvate or lactic acid. On immediate collection from the cauda epididymidis, it was observed that ATP levels in spermatozoa derived from *Pkm*-vKO males were merely 6.3% of the levels measured in control cells (**Figure 3a**). To exclude the possibility of sperm death resulting in the loss of motility, we also assessed sperm viability. The remarkably diminished ATP levels observed in spermatozoa from *Pkm*-vKO mice were likely accountable for the observed absence of progressive motility. This inference is substantiated by the fact that sperm viability remained consistent between control and *Pkm*-vKO males (**Figure 3b**).

### *Loss of sperm PKM and capacitation-associated phosphorylation and the acrosome reaction*

Protein kinase A-dependent tyrosine phosphorylation of a distinct subset of sperm proteins stands as a crucial molecular indicator of capacitation, intricately connected to modifications in sperm function.[24,29,32] By utilizing western blot and a specific anti-phosphotyrosine antibody, the anticipated augmented pattern of phosphorylated proteins was discerned when wild-type spermatozoa underwent 90 min of *in vitro* capacitation within HMB medium, void of pyruvate or lactic acid. However, in contrast, spermatozoa devoid of PKM demonstrated no upsurge in tyrosine phosphorylation when exposed to identical conditions (**Figure 5a**).

Furthermore, the capability of *Pkm*-vKO spermatozoa to undergo the acrosome reaction, a pivotal phase in fertilization, was examined. This reaction, reliant on calcium ($Ca^{2+}$), involves exocytosis and can be prompted *in vitro* by the $Ca^{2+}$ ionophore A23187, progesterone (P4), or solubilized zonae pellucidae. Intriguingly, spermatozoa lacking PKM showed no deficiencies in A23187 or P4-induced acrosome reactions when juxtaposed with their wild-type counterparts (**Figure 5b**).

### *PKM and sperm-egg interaction*

In order to delve deeper into the assessment of the fertilization potential of epididymal *Pkm*-vKO spermatozoa, we undertook an IVF analysis. Through this analysis, we ascertained the ratio of two-cell embryos to the overall count of oocytes. The results showed that spermatozoa from *Pkm*-vKO mice had a significantly lower fertilization rate compared with wild-type sperm, indicating that PKM in sperm is crucial for

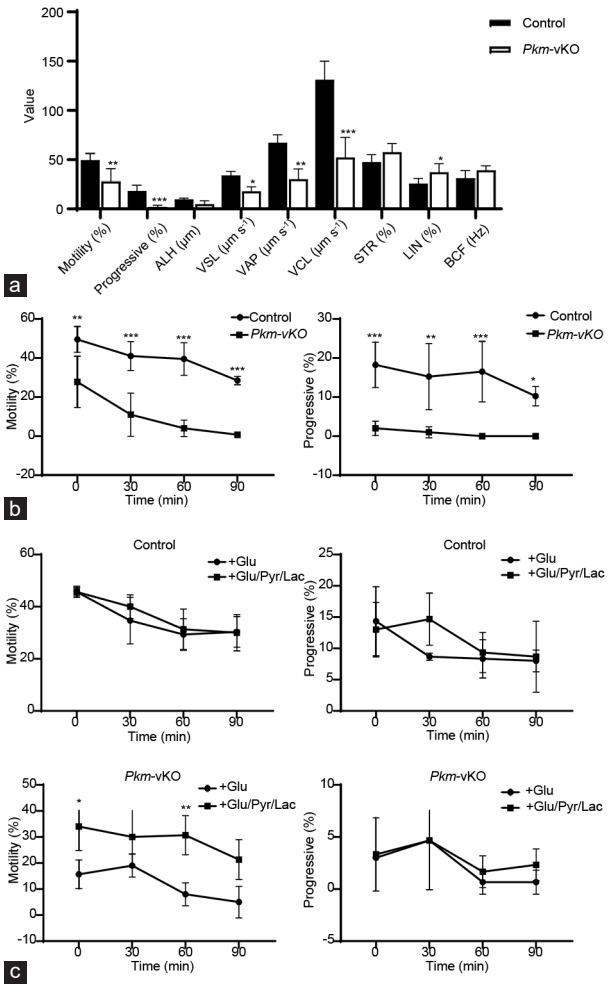


**Figure 4:** *Pkm* knockout impairs sperm motility. (**a**) Computer-assisted sperm analysis (CASA) was used to evaluate sperm motility parameters immediately after collection ($n = 4$). The data are shown as mean ± standard deviation. (**b**) Percentage of motile (left) and progressive (right) sperm from control and *Pkm*-vKO mice in glucose-only capacitation medium ($n = 4$). (**c**) Percentage change of total motile (left) and progressively motile (right) spermatozoa from control and *Pkm*-vKO mice ($n$=3 for each group) in the medium with or without pyruvate and lactate supplementation. Results are presented as mean ± standard deviation. $^{*}P < 0.05$, $^{**}P < 0.01$, $^{***}P < 0.001$. The $P$ value was calculated by two-tailed Student's $t$-test. PKM: pyruvate kinase M; *Pkm*-vKO: germ cell-specific *Pkm* gene knockout; VCL: curvilinear velocity; VAP: average path velocity; VSL: straight-line velocity; ALH: amplitude of lateral head displacement; STR: straightness rate; BCF: beat cross frequency; LIN: linearity; Glu: glucose; Pyr: pyruvate; Lac: lactate.

the interaction between spermatozoon and oocyte for successful fertilization (**Figure 6**).

## DISCUSSION

Normal spermatogenesis demands a substantial energy reservoir. While glycolysis is a pivotal avenue for ATP generation, its efficiency is limited, producing just 2 ATP molecules per glucose unit. Hence, OXPHOS is pivotal for generating a significant ATP yield. The absence of PKM hinders the production of pyruvate, consequently impeding its entry into the tricarboxylic acid (TCA) cycle sans external supplementation. Our findings suggest that PKM within spermatogenic cells is not obligatory for spermatogenesis, as its removal via *Vasa-Cre* in mice did not disrupt the process. This prompts inquiries about the energy provisioning mechanism for supporting spermatogenesis. A plausible explanation is that pyruvate or intermediates yielded through glycolysis and OXPHOS by adjacent Sertoli cells may traverse into spermatogenic cells, orchestrating the entire spermatogenic progression, which includes spanning stem cell mitosis, spermatocyte meiosis, and round spermatid spermiogenesis. Prior investigations have posited that the interplay between Sertoli cells and germ cells elicits germ cell differentiation under *in vitro* conditions.[33,34] The significance of exogenous lactate in the metabolic processes of distinct spermatocytes and spermatids has been proposed, serving as a crucial energy source for the maturation of germ cells. Furthermore, Sertoli cells display the capability to offer an additional supply of lactate.[11,35-38] Sertoli cells possess the ability to metabolize a range of substrates, with glucose emerging as the favored option. However, it is worth noting that a significant portion of glucose undergoes conversion into lactate instead of being oxidized through the TCA cycle.[37] However, SSCs reside within a hypoxic, avascular setting, and an elevated glycolytic activity substantiates the prolonged self-renewal capabilities of SSCs.[9,10] The absence of noticeable effects on both SSCs and the entire spermatogenesis process following PKM disruption is intriguing, especially considering the distinct expression of PKM in spermatogonia and spermatids compared to spermatocytes, as indicated by our mouse testicular single-cell RNA sequencing data. Subsequent investigations will be instrumental in uncovering the mechanisms that uphold SSC self-renewal among PKM dysfunction.

Sperm motility and capacitation demand substantial ATP consumption, with sperm cells exhibiting unique bioenergetic characteristics. Glycolysis takes place within the principal piece of spermatozoa, while OXPHOS occurs within the mitochondria-rich midpiece.[11,12] Research indicates the indispensability of glycolysis for the motility of mouse sperm.[15] Mice lacking various sperm-specific glycolytic enzymes (glyceraldehyde-3-phosphate dehydrogenase, spermatogenic [GAPDHS], phosphoglycerate kinase 2 [PGK2], and lactate dehydrogenase C [LDHC]) demonstrate compromised male fertility characterized by reduced sperm motility and diminished ATP levels. However, the observed phenotypes in these mice exhibit certain variations. For instance, male mice deficient in PGK2 or LDHC exhibit subfertility, whereas those lacking GAPDHS are rendered infertile. Furthermore, male mice devoid of PGK2 or LDHC showcase higher initial motility and ATP levels compared to their GAPDHS-deficient counterparts.[16,39,40] The more pronounced phenotype observed in mice lacking GAPDHS, in comparison to those lacking PGK2, could be attributed to reduced protein phosphatase 1 phosphorylation, elevated metabolite levels, and the absence of progressive motility on exposure to pyruvate as the exclusive metabolic substrate in GAPDHS-deficient mouse sperm.[29] The results from our *Pkm*-vKO mice also support the importance of glycolysis for sperm motility and exhibit similar results, with male infertility, sperm motility defects, and low ATP levels. Exogenous pyruvate and lactic acid supplementation can partially rescue the total motility impairment, but it fails to improve the progressive movement of the spermatozoa without PKM. The possible explanation for this phenomenon is that ATP produced in the mitochondria cannot be efficiently transported from the midpiece to the principal piece to support flagellum beating.[15] We measured ATP levels in the absence or presence of pyruvate and lactate. The findings revealed that after the introduction of pyruvate and lactate, the ATP concentrations within the knockout cohort exhibited a discernible elevation in relation to the control cohort. Nevertheless, the ATP levels failed to attain restitution to the analogous levels observed in the control group (**Supplementary Figure 4**). From these findings, it appears that both glycolysis and OXPHOS play a crucial role in maintaining sperm

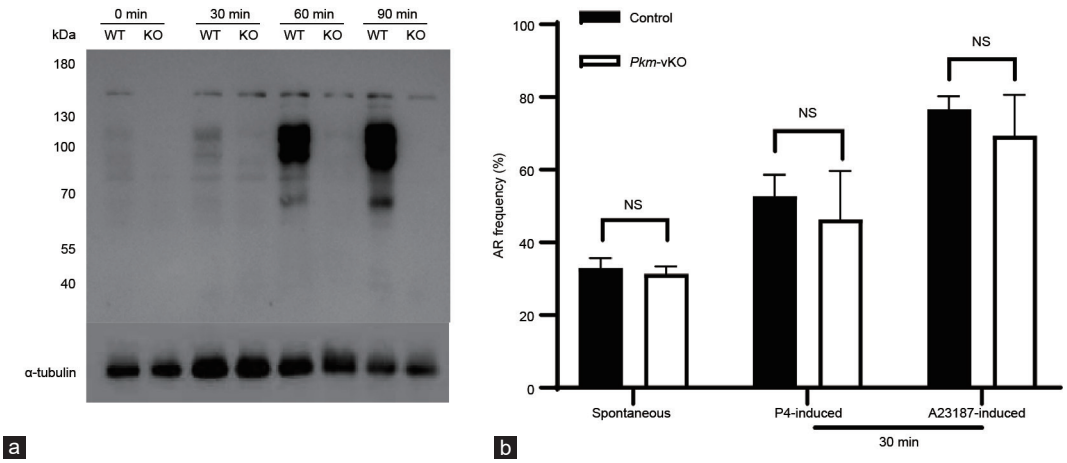


**Figure 5:** Evaluation of alterations in protein tyrosine phosphorylation during sperm capacitation, coupled with the evaluation of sperm acrosome reaction rates in control and *Pkm*-vKO mice. (**a**) Quantification of protein tyrosine phosphorylation associated with capacitation in spermatozoa from both control (WT) and *Pkm*-vKO (KO) mice. (**b**) Comparative analysis of the frequency of spontaneous and P4/A23187-induced acrosome reactions between sperm from control and *Pkm*-vKO mice ($n$ = 3). Results are depicted as mean ± standard deviation. The statistical significance was determined using a two-tailed Student's *t*-test. NS: nonsignificant. WT: wildtype; KO: knockout; *Pkm*-vKO: germ cell-specific *Pkm* gene knockout; AR: acrosomal reaction.

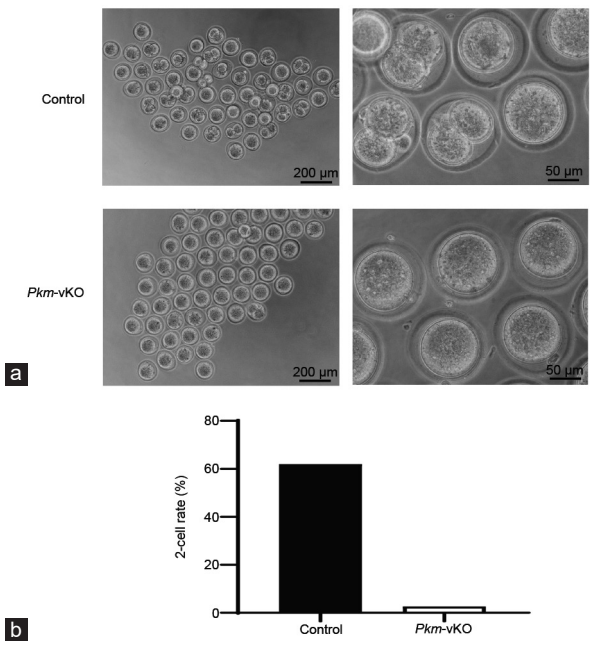


**Figure 6:** Examination of the fertilization capability of sperm from control and *Pkm*-vKO mice. (**a**) Illustrative depictions showcasing oocytes and two-cell embryos. (**b**) *In vitro* fertilization investigation involving spermatozoa from both control and *Pkm*-vKO mice, utilizing intact oocytes ($n$ = 2). The outcomes are exhibited in mean values. *Pkm*-vKO: germ cell-specific *Pkm* gene knockout.

motility, with glycolysis being the dominant pathway. It is interesting that spermatozoa lacking PKM demonstrated no deficiencies in ionophore or progesterone-induced acrosome reactions despite impaired IVF compared with wild-type sperm. Similar phenomenon has been reported for *Gapds* or *Pgk2* knockout mice.[29] Furthermore, existing literature indicates that spermatozoa subjected to a state of deprivation (medium lacking energy nutrients) exhibit a markedly augmented propensity to undergo a progesterone-induced acrosome reaction.[41]

In conclusion, our study has revealed that the absence of PKM does not lead to the changes in testicular histology, sperm counts, or sperm morphology. However, PKM plays a crucial role in maintaining typical sperm motility, facilitating protein tyrosine phosphorylation during sperm capacitation, and promoting effective sperm-egg interaction. To our understanding, this marks the inaugural unveiling of PKM's significance in both spermatogenesis and sperm motility. However, further investigations are imperative to comprehend the mechanisms underlying the preserved normalcy of spermatogenesis post the loss of PKM.

## AUTHOR CONTRIBUTIONS

QL and BS conceived and designed the study. GQQ, XCW, and XZ performed the experiments. GQQ and QL drafted the manuscript. All authors read and approved the final manuscript.

## COMPETING INTERESTS

All authors declare no competing interests.

## ACKNOWLEDGMENTS

The study was supported by the National Natural Science Foundation of China (No. 81571488 and No. 81771637). We thank Prof. Ming-Han Tong from Shanghai Institute of Biochemistry and Cell Biology (Shanghai, China) for his active instruction and kind support and suggestion in this work.

Supplementary Information is linked to the online version of the paper on the *Asian Journal of Andrology* website.

## REFERENCES

1 Griswold MD. Spermatogenesis: the commitment to meiosis. *Physiol Rev* 2016; 96: 1–17.
2 Xi HM, Ren YJ, Ren F, Li Y, Feng TY, *et al*. Recent advances in isolation, identification, and culture of mammalian spermatogonial stem cells. *Asian J Androl* 2022; 24: 5–14.
3 Lin Z, Hsu PJ, Xing X, Fang J, Lu Z, *et al*. *Mettl3-/Mettl14*-mediated mRNA N(6)-methyladenosine modulates murine spermatogenesis. *Cell Res* 2017; 27: 1216–30.
4 Wang T, Yin Q, Ma X, Tong MH, Zhou Y. *Ccdc87* is critical for sperm function and male fertility. *Biol Reprod* 2018; 99: 817–27.
5 Sullivan R, Mieusset R. The human epididymis: its function in sperm maturation. *Hum Reprod Update* 2016; 22: 574–87.
6 Björkgren I, Sipilä P. The impact of epididymal proteins on sperm function. *Reproduction* 2019; 158: R155–67.
7 Gervasi MG, Visconti PE. Chang's meaning of capacitation: a molecular perspective. *Mol Reprod Dev* 2016; 83: 860–74.
8 Okabe M. The cell biology of mammalian fertilization. *Development* 2013; 140: 4471–9.
9 Lord T, Nixon B. Metabolic changes accompanying spermatogonial stem cell differentiation. *Dev Cell* 2020; 52: 399–411.

10 Zhang Z, Miao J, Wang Y. Mitochondrial regulation in spermatogenesis. *Reproduction* 2022; 163: R55–69.
11 Park YJ, Pang MG. Mitochondrial functionality in male fertility: from spermatogenesis to fertilization. *Antioxidants (Basel)* 2021; 10: 98.
12 Amaral A. Energy metabolism in mammalian sperm motility. *WIREs Mech Dis* 2022; 14: e1569.
13 Ford WC. Glycolysis and sperm motility: does a spoonful of sugar help the flagellum go round? *Hum Reprod Update* 2006; 12: 269–74.
14 Storey BT. Mammalian sperm metabolism: oxygen and sugar, friend and foe. *Int J Dev Biol* 2008; 52: 427–37.
15 Mukai C, Okuno M. Glycolysis plays a major role for adenosine triphosphate supplementation in mouse sperm flagellar movement. *Biol Reprod* 2004; 71: 540–7.
16 Miki K, Qu W, Goulding EH, Willis WD, Bunch DO, *et al*. Glyceraldehyde 3-phosphate dehydrogenase-S, a sperm-specific glycolytic enzyme, is required for sperm motility and male fertility. *Proc Natl Acad Sci U S A* 2004; 101: 16501–6.
17 Chen Y, Zheng Y, Gao Y, Lin Z, Yang S, *et al*. Single-cell RNA-seq uncovers dynamic processes and critical regulators in mouse spermatogenesis. *Cell Res* 2018; 28: 879–96.
18 Schormann N, Hayden KL, Lee P, Banerjee S, Chattopadhyay D. An overview of structure, function, and regulation of pyruvate kinases. *Protein Sci* 2019; 28: 1771–84.
19 Lee YB, Min JK, Kim JG, Cap KC, Islam R, *et al*. Multiple functions of pyruvate kinase M2 in various cell types. *J Cell Physiol* 2022; 237: 128–48.
20 Zheng S, Liu Q, Liu T, Lu X. Posttranslational modification of pyruvate kinase type M2 (PKM2): novel regulation of its biological roles to be further discovered. *J Physiol Biochem* 2021; 77: 355–63.
21 Alquraishi M, Puckett DL, Alani DS, Humidat AS, Frankel VD, *et al*. Pyruvate kinase M2: a simple molecule with complex functions. *Free Radic Biol Med* 2019; 143: 176–92.
22 Yang W, Lu Z. Pyruvate kinase M2 at a glance. *J Cell Sci* 2015; 128: 1655–60.
23 Pietrobon EO, Domínguez LA, Vincenti AE, Burgos MH, Fornés MW. Detection of the mouse acrosome reaction by acid phosphatase. Comparison with chlortetracycline and electron microscopy. *J Androl* 2001; 22: 96–103.
24 Visconti PE, Bailey JL, Moore GD, Pan D, Olds-Clarke P, *et al*. Capacitation of mouse spermatozoa. I. Correlation between the capacitation state and protein tyrosine phosphorylation. *Development* 1995; 121: 1129–37.
25 Chen Y, Ma L, Hogarth C, Wei G, Griswold MD, *et al*. Retinoid signaling controls spermatogonial differentiation by regulating expression of replication-dependent core histone genes. *Development* 2016; 143: 1502–11.
26 Xia X, Wang L, Yang X, Hu Y, Liu Q. Acute damage to the sperm quality and spermatogenesis in male mice exposed to curcumin-loaded nanoparticles. *Int J Nanomedicine* 2020; 15: 1853–62.
27 World Health Organization. WHO Laboratory Manual for the Examination and Processing of Human Semen. 5th ed. Geneva: World Health Organization; 2010. p271.
28 Moller CC, Bleil JD, Kinloch RA, Wassarman PM. Structural and functional relationships between mouse and hamster zona pellucida glycoproteins. *Dev Biol* 1990; 137: 276–86.
29 Huang Z, Danshina PV, Mohr K, Qu W, Goodson SG, *et al*. Sperm function, protein phosphorylation, and metabolism differ in mice lacking successive sperm-specific glycolytic enzymes. *Biol Reprod* 2017; 97: 586–97.
30 Yin Q, Shen J, Wan X, Liu Q, Zhou Y, *et al*. Impaired sperm maturation in conditional *Lcn6* knockout mice. *Biol Reprod* 2018; 98: 28–41.
31 Gallardo T, Shirley L, John GB, Castrillon DH. Generation of a germ cell-specific mouse transgenic Cre line, *Vasa-Cre*. *Genesis* 2007; 45: 413–7.
32 Visconti PE, Moore GD, Bailey JL, Leclerc P, Connors SA, *et al*. Capacitation of mouse spermatozoa. II. Protein tyrosine phosphorylation and capacitation are regulated by a cAMP-dependent pathway. *Development* 1995; 121: 1139–50.
33 Ziparo E, Geremia R, Russo MA, Stefanini M. Surface interaction *in vitro* between Sertoli cells and germ cells at different stages of spermatogenesis. *Am J Anat* 1980; 159: 385–8.
34 Tres LL, Kierszenbaum AL. Viability of rat spermatogenic cells *in vitro* is facilitated by their coculture with Sertoli cells in serum-free hormone-supplemented medium. *Proc Natl Acad Sci U S A* 1983; 80: 3377–81.
35 Courtens JL, Plöen L. Improvement of spermatogenesis in adult cryptorchid rat testis by intratesticular infusion of lactate. *Biol Reprod* 1999; 61: 154–61.
36 Boussouar F, Benahmed M. Lactate and energy metabolism in male germ cells. *Trends Endocrinol Metab* 2004; 15: 345–50.
37 Rato L, Alves MG, Socorro S, Duarte AI, Cavaco JE, *et al*. Metabolic regulation is important for spermatogenesis. *Nat Rev Urol* 2012; 9: 330–8.
38 Jutte NH, Grootegoed JA, Rommerts FF, van der Molen HJ. Exogenous lactate is essential for metabolic activities in isolated rat spermatocytes and spermatids. *J Reprod Fertil* 1981; 62: 399–405.
39 Odet F, Duan C, Willis WD, Goulding EH, Kung A, *et al*. Expression of the gene for mouse lactate dehydrogenase C (*Ldhc*) is required for male fertility. *Biol Reprod* 2008; 79: 26–34.
40 Danshina PV, Geyer CB, Dai Q, Goulding EH, Willis WD, *et al*. Phosphoglycerate kinase 2 (PGK2) is essential for sperm function and male fertility in mice. *Biol Reprod* 2010; 82: 136–45.
41 Sánchez-Cárdenas C, Romarowski A, Orta G, De la Vega-Beltrán JL, Martín-Hidalgo D, *et al*. Starvation induces an increase in intracellular calcium and potentiates the progesterone-induced mouse sperm acrosome reaction. *FASEB J* 2021; 35: e21528.

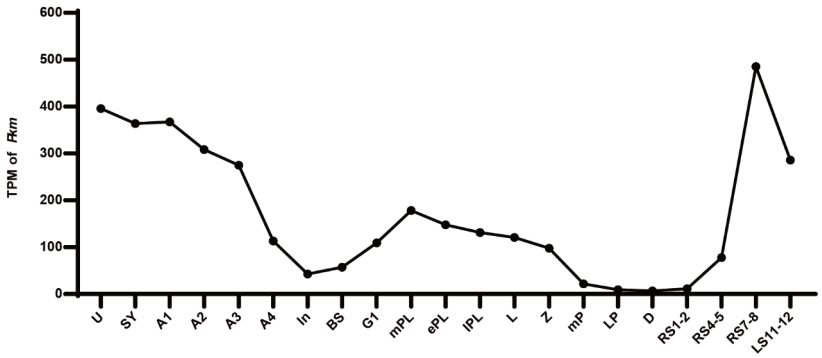


**Supplementary Figure 1:** Dynamic fluctuations in *Pkm* transcripts were observed across various levels of spermatogenic cells within the testes. This insight was achieved by initiating the dissociation of testes into a single-cell suspension, followed by population-level sorting through FACS. Through the application of the Unipick system, single cells were meticulously selected based on their fluorescence and cell size attributes. In total, a comprehensive profiling of twenty spermatogenic cell subtypes was undertaken, encompassing undifferentiated spermatogonia (U), synchronization (SY), differentiated spermatogonia (A1: type A1 spermatogonia, A2: type A2 spermatogonia, A3: type A3 spermatogonia, A4: type A4 spermatogonia, In: intermediate spermatogonia, BS: S phase type B spermatogonia), preleptotene spermatocytes (G1: G1 phase preleptotene; ePL: early S phase preleptotene; mPL: middle S phase preleptotene; lPL: late S phase preleptotene), meiotic cells (L: leptotene; Z: zygotene; mP: middle pachytene; lP: late pachytene; D: diplotene), and round spermatids (RS1-2: steps 1-2 spermatids; RS3-4: steps 3-4 spermatids; RS5-6: steps 5-6 spermatids; RS7-8: steps 7-8 spermatids; LS11-12: steps 11-12 spermatids).

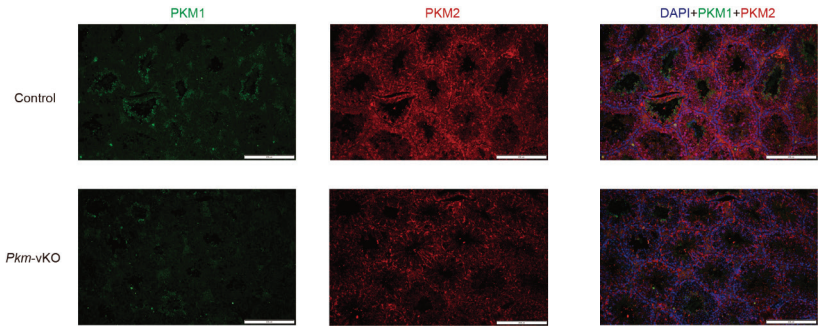


**Supplementary Figure 2:** Immunostaining of PKM1 and PKM2 in the testes of control and *Pkm*-vKO mice is depicted. The images visually capture the immunostaining process, highlighting PKM1 (green), PKM2 (red), and DAPI (blue) within the mouse testes. (Scale bars: 200 μm).

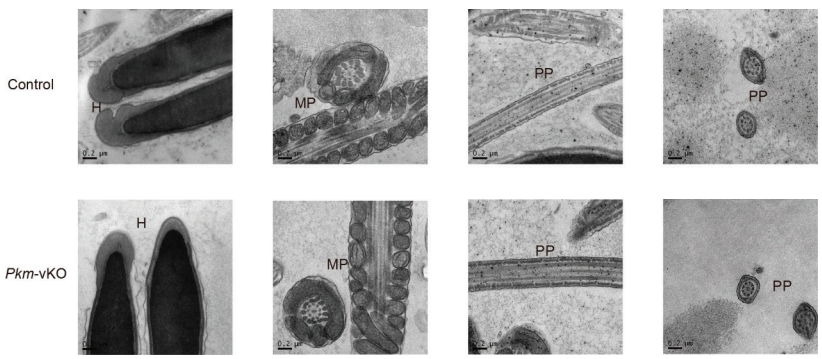


**Supplementary Figure 3:** Morphological analysis of control and *Pkm*-vKO sperm using transmission electron microscopy. H: head; MP: midpiece; PP: principal piece. Scale bar: 0.2 μm.

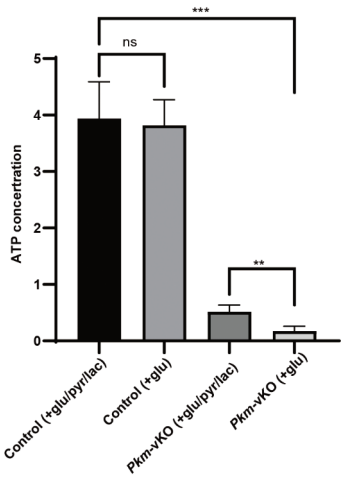


**Supplementary Figure 4:** Sperm ATP levels were assessed in HMB medium, both in the presence and absence of pyruvate and lactic acid. In the control, the ATP concentration remained relatively stable before and after the introduction of acetate and lactate, exhibiting no significant alterations. Conversely, within the *Pkm*-vKO sperm, the addition of acetate and lactate led to a discernible rise in ATP concentration, although not reaching the level observed in the control. ATP: Adenosine Triphosphate Results are presented as means ± s.d (Control, $n = 3$; *Pkm*-vKO, $n = 4$). ns: non-significant, Glu: Glucose; Pyr: pyruvate; Lac: lactate. $^{**}P < 0.01$, $^{***}P < 0.001$. The $P$ value was calculated by two-tailed Student's *t*-test.